The Use of Extra-Galactic Star Formation Tracers on Star Forming Regions in the Milky Way

APPROVED BY

SUPERVISING COMMITTEE:

Neal J. Evans II, Supervisor

John Lacy

The Use of Extra-Galactic Star Formation Tracers on Star Forming Regions in the Milky Way

by

Nalin Vutisalchavakul, B.A.

THESIS

Presented to the Faculty of the Graduate School of

The University of Texas at Austin

in Partial Fulfillment

of the Requirements

for the Degree of

MASTER OF ARTS

THE UNIVERSITY OF TEXAS AT AUSTIN

August 2011

Dedicated to my family and my teacher Robert O. Harmon.

Acknowledgments

I would like to thank many people who have helped me throughout my work. First of all, I would like to thank my advisor Neal Evans for guiding me through the project. I would also like to thank my research committee, the star formation group, and everyone at the department of astronomy for all the support and helpful comments. I am also grateful for the help from George Helou, whose suggestions were a big part of the development of this project.

The Use of Extra-Galactic Star Formation Tracers on Star Forming Regions in the Milky Way

Nalin Vutisalchavakul, M.A.
The University of Texas at Austin, 2011

Supervisor: Neal J. Evans II

We studied three groups of star forming clouds in the Milky Way: 5 clouds from Spitzer c2d Legacy survey, 10 clouds from Gould Belt survey, and 32 massive dense clumps. We determined the total diffuse $24\mu m$ emission for each cloud and calculated the corresponding SFR using an extragalactic relation. Then the resulting SFRs were compared with SFRs calculated using the method of counting number of YSOs for c2d and Gould Belt clouds and using L_{IR} for massive dense clumps. The comparison shows quite a good correlation for the massive dense clumps, which are high-mass star forming regions, with the average ratio of $SFR(L_{IR})/SFR(25\mu m) = 0.896 \pm 0.663$. The result for low-mass star forming clouds (c2d and Gould Belt) shows very little to no correlation between $L_{24\mu m}$ and SFR(YSO count). Comparing $24\mu m$ images with extinction maps shows that a significant portion of $24\mu m$ emission does not come from star-forming regions in the cloud.

Table of Contents

List of Tables

List of Figures

Chapter 1

Introduction

Star formation in galaxies is an important subject that has been studied by numerous surveys. It is evident from many studies that star formation properties vary depending on types and other features of galaxies (Kennicutt 1998, Bigiel 2008, Gao 2004). Understanding star formation properties and histories over different types of galaxies would help us in the study of galaxy formation and evolution (Kennicutt 1998, Bigiel 2008). Since most galaxies are too far away for individual star forming regions to be resolved, systematic and reliable observational techniques for probing star formation properties are needed. There are many different methods that have been used to estimate star formation rate (SFR) in galaxies. Common tracers include continuum UV emission, recombination lines of Hydrogen and other atomic species, total infrared luminosity, monochromatic infrared emission, and radio emission (Kennicutt 1998, 2003; Evans 2003; Kinney 1993; Condon 1992). Each of these tracers traces different component of the star forming regions. UV continuum emission in the wavelength range of 125-250 nm includes radiation from high mass stars while hydrogen recombination lines such as H-α trace emission from HII regions surrounding high mass stars (Kennicutt 1998). Infrared emission traces emission from dust grains that have been heated by stellar

photons (Calzetti 2007, Evans 2003). Radio emission can be contributed by synchrotron and free-free emission, which has been emitted by electrons in HII regions (Condon 1992).

Many galaxy surveys used UV and optical lines as tracers of SFR (Begiel 2008, Kinney 1993). For star forming regions that are obscured by dust, however, UV and optical lines are not effective tracers due to the fact that both are heavily affected by dust-extinction (Calzetti 1994). As supplements to UV and optical tracers, IR fluxes have been used to study SFR in regions that are obscured by dust (Calzetti 2007). While hydrogen recombination lines are supposed to trace the number of ionizing photons radiated from young stars that have been reemitted by hydrogen in the HII regions, infrared dust emission is supposed to trace the number of stellar photons that have been absorbed by dust and reemitted in the infrared (Calzetti 2007, Evans 2003). If all the photons inside star forming regions get absorbed by dust, then L_{IR} from dust should indirectly trace amount of photons from the stars. One implication of using L_{IR} to trace star formation is that sources other than young stars could contribute to heating the dust. For some galaxies, a significant amount of dust heating could come from older stellar populations (Kennicutt 1998, Draine 2007). In that case, L_{IR} would trace emission that is not relevant to the current star formation. Other than using L_{IR}, monochromatic IR emission can also be used. One particular tracer used for studying SFR in HII regions for numerous galaxies is the $24\mu m$ continuum emission (Calzetti 2007, Wu 2005). One probable advantage of using $24\mu m$ instead of L_{IR} as

a tracer is that emission in $24\mu m$ should come from warm dust. The diffuse part of the interstellar medium that has been heated by average interstellar radiation field should be at a comparatively low temperature and do not emit much in the $24\mu m$ wavelength band compare to the emission from high mass star forming regions. Stronger radiation field from high mass stars can heat the dust to higher temperature; therefore, $24\mu m$ emission should be a good tracer for high mass star forming regions with less contamination from non-star-forming sources. There are several studies of how emission from non-star-forming sources compare to emission relevant to star formation in the $24\mu m$ wavelength (Rahman 2011, Verley 2008, Draine 2007). Draine et al. showed from fitting dust-models to numbers of galaxies that for galaxies with high star formation rates (starburst galaxies), the main contribution in $24\mu m$ emission comes from photodissociation regions associated with high mass stars. For high mass star forming regions, $24\mu m$ emission should be a good tracer of SFR.

In order to test how well $24\mu m$ emission can trace SFR, another method for tracing SFR is needed for comparison. The goal of our study is to compare SFR calculated from $24\mu m$ -SFR relation with SFR calculated using a different method for star forming clouds in the Milky Way. Our study includes both low mass and high mass star forming regions. Since we can look at more details of star forming regions in the Milky Way, testing extragalactic SFR relation on nearby regions could provide us a better understanding of how well $24\mu m$ can trace SFR and if the results are different for low mass and high mass star

forming regions.

In this study, we selected samples of molecular clouds in the Milky Way to study the SFR calculated using $24\mu m$ flux. In section 2 we describe how the SFR was calculated for a sample of nearby molecular clouds from the Spitzer c2d (core to disk) Legacy project and from survey of Gould's Belt clouds. In section 3, we show the study of high mass star forming regions using samples of massive, dense, clumps from Wu et al. (2010). The resulting comparison of all the SFRs in this study is described in section 4. And the summary of this study is described in section 5.

Chapter 2

24μm emission of low mass star forming clouds

The first two groups of molecular clouds we looked at were clouds from the Spitzer c2d LEGACY project and Gould's Belt survey. These clouds are nearby, low mass star forming clouds. Spitzer c2d survey observed Chamaeleon II, Serpens, Perseus, Ophiuchus, and Lupus I, III, and IV. They lie within 300 pc of the Sun. From the c2d LEGACY project, these clouds have been observed in the IRAC bands (3.6, 4.5, 5.6, 8.0 μm) and MIPS bands (24, 70, 160 μm) (Evans et al. 2009). The second group of molecular clouds we studied was a part of Spitzer Gould Belt cloud survey (Allen et al. in prep). The clouds we studied consist of Auriga North, Auriga, Cepheus, Chamaeleon I, Chamaeleon III, Corona Australis (CrA), IC5146, Lupus VI, Lupus V, Musca, and Scorpius. They are parts of Gould Belt, a ring on the sky containing many star forming regions. The survey observed these clouds in the same IRAC and MIPS bands as the c2d survey. From the data on the fluxes, Young Stellar Objects (YSOs) were identified in each cloud and categorized by their SED classes. The same procedures for identifying YSOs and calculating SFR were performed on both c2d and Gould's Belt clouds. The details on identifying YSOs and calculating SFR in these clouds can be found in Evans et al. 2009. There are a total of 1024 YSOs combined for the five c2d clouds. Numbers of YSOs in each

individual cloud are listed in Table 1.

Our goal is to compare star formation rates (SFR) calculated using $24\mu m$ flux with SFR obtained using another method to see if the $24\mu m$- SFR relation work for low mass star forming clouds in the Milky Way. The SFR we can use for comparison has been calculated in Evans et al. (2009) for the c2d survey and Allen et al (in prep). SFRs for Gould's Belt survey is also available in Heiderman et al (2010). After identifying YSOs and their SED classes, the SFR can be estimated by assuming an average mass of $0.5M_{\odot}$ for each YSO and an average time for YSOs to go through SED class II of 2 Myr. The SFR can then be calculated by SFR = (Average mass)$\times$(Number of YSOs) / (lifetime of class II) (Evans et al. 2009). The estimated SFR for each cloud are included in Table 1 with Perseus having the highest SFR followed by Ophiuchus.

2.1 $24\mu m$ emission from YSOs

We are interested in the $24\mu m$ flux data from the MIPS bands. The 24 μm images are available for all of the clouds observed. The flux for individual YSO is also listed in the c2d data catalogue. We first extracted all the objects labeled as YSOs along with their respective 24 μm fluxes. Then we summed over the flux for all the YSOs in individual clouds. The resulting total YSO fluxe for each cloud is shown in Table 2.1.

The 24 μm - SFR correlation for extragalactic star formation has been derived in a number of studies (Calzetti 2007, Alonso-Herrero st al. 2006).

The calibration we used in this study came from the work of Calzetti et al. (2007), which stated that the 24 μm luminosity traces SFR by

$$\mathrm{SFR}(M_\odot\ \mathrm{yr}^{-1}) = 1.27 \times 10^{-38}[L_{24\,\mu m}(\mathrm{ergs\ s}^{-1})]^{0.8850}, \qquad (2.1)$$

where $L_{24\,\mu m}$ is the total 24 μm luminosity times the frequency (νL_ν) (Calzetti et al. 2007). The calculated SFRs for each cloud are as shown in Table 2.1.

A comparison between SFRs calculated from the 24μm YSOs flux (SFR(YSO, 24 μm)) with SFRs from counting YSOs (SFR(YSO count)) indicates that our calculated SFR(YSO, 24 μm) are much smaller than SFR(YSO count) with the mean ratio SFR(YSO count)/SFR(YSO, 24μm) of 1867$\pm$1335.

2.2 24μm diffuse emission

Since the relation was derived for extra-galactic star formation, we might expect the detected flux to be contributed from diffuse emission as well as from point sources. Using only the flux from YSOs could omit a large portion of the flux. For further analysis, the diffuse emission should also be included in the SFR calculation.

The c2d and Gould's Belt clouds survey include 24 μm MIPS images for the full observed regions of each cloud. Our goal was first to obtain the total flux for the whole region of the cloud as observed by MIPS 24 μm band. The images for each cloud were analyzed to sum over all the pixel values of the image. After obtaining the fluxes, the SFRs for each cloud were calculated using the same 24μm-SFR relation shown in equation (2.1). The resulting flux

Table 2.1. SFR for the c2d and Gould's Belt clouds

Cloud -	Distance (pc)	NYSOs -	YSO Flux (Jy)	SFR (YSO, 24 μm) ($M_\odot$ Myr^{-1})	SFR (YSO count) ($M_\odot$ Myr^{-1})	SFR(YSO count)/SFR(YSO, 24 μm) -
PER	250	385	77.1	0.090	96	1070
CHA II	178	24	7.93	0.0066	6.5	989
OPH	125	290	94.2	0.031	73	2330
SER	260	224	56.7	0.073	57	778
LUP	150	93	9.45	0.0057	24	4230
AUR	300	173	26.5	0.048	43.3	902
CEP	300	118	24.5	0.045	29.5	656
CHA I	200	89	-	-	22.2	-
CHA III	200	4	0.254	0.00038	1.0	2630
CrA	130	41	11.9	0.0054	10.2	1890
IC5146	950	131	16.9	0.25	32.7	131
LUP V	150	43	5.14	0.0033	10.8	3270
LUP VI	150	45	6.67	0.0042	11.2	2670
MUSCA	160	12	0.839	0.00075	3.0	4000
SCO	130	10	8.88	0.0042	2.5	595

for each cloud and the corresponding SFRs are shown in table 2.2. The ratios of SFR/SFR(24,diffuse) are close to one with the mean of 2.11±2.00 for c2d clouds and 1.224±1.264 for Gould's Belt clouds. The median is 1.76±1.79 and 0.962±1.218 for c2d and Gould's Belt clouds respectively.

From the preliminary calculations of the total diffuse flux , it is evident that the fluxes for all the clouds are significantly higher than the flux from YSOs. The resulting SFR(24, diffuse)s are also much closer to the c2d calculation than the SFR calculated from YSOs flux alone. There are some uncertainties in the calculation. One source of uncertainty comes from the uncertainties in the measured distance to the cloud. There is evidence that each Lupus cloud maybe at a different distance (Evans et al. 2009). The diffuse flux calculation of Ophiuchus cloud was obtained from a single, combined image of the cloud (Ophiuchus and Ophiuchus North).

After the preliminary estimation of the total diffuse flux, more careful calculations were performed on each cloud. To be able to compare SFR from diffuse 24 μm emission with SFR from counting YSOs, the calculations have to come from the same area of the clouds. MIPS 24 μm maps generally cover much larger areas of the clouds than the areas used in classifying YSOs. Boundaries for each clouds used in classifying YSOs were chosen using contours from extinction maps. Therefore, we confined our areas of the clouds for calculating diffuse emission to areas inside the same extinction contours used in classifying YSOs. All clouds' boundaries were chosen to be extinction contours of $A_V = 2$ except for Serpens with $A_V = 6$ and Ophiuchus with $A_V = 3$

(Evans 2007). The total flux used in calculating SFR should also be emission only from the clouds themselves. MIPS images contain flux from the area observed; the total flux includes emission from the cloud as well as extended background emission. To only include flux from the clouds, we need to subtract background emission from the images. Since these clouds are extended objects with no distinct boundaries, background subtraction is not simple. There are several ways to estimate background emission. First, off-cloud images, which are images taken of the area of the sky near the clouds, can be used to estimate the background level. There are off-cloud images only for three clouds: Lupus, Ophiuchus, and Serpens. We calculated the average flux per pixel (Jy/pixel) from these off cloud images for the three clouds for comparisons. Since we defined boundaries for all the clouds using extinction countours, area of clouds outside of the contours can be used as backgrounds. There were few problems with this method of calculating background emission. One of the problem is that not all the clouds have the same extinction contour levels as boundaries. Extinction maps for Serpens and Ophiuchus do not cover down to $A_V = 2$ level, which is why the contour levels chosen as boundaries for these two clouds are different from the rest of the clouds. Using areas outside of contour boundaries as background would then include up to different density levels for different clouds. From looking at MIPS images, there are still some regions with strong emission outside of the boundaries. Considering all area outside of the boundaries as background could also overestimate background levels if there is still some emission from the cloud within the area. The last method

of estimating background level we considered was by averaging pixel values from area of the images far from the clouds' centers. We looked at each cloud image and picked regions near the edge of the image that does not seem to contain bright emission and averaged over those pixels to obtain the background level. As long as the fluxes are averaged over large number of pixels, this method should provide the most consistent background estimations for all the clouds. We then used the background levels calculated by this method for background subtraction. The total flux inside contour boundaries minus the background flux (background flux = average background level per pixel $\times$ number of pixels inside the boundary) gave actual flux from the clouds. The background subtracted fluxes inside contour boundaries for each cloud are shown in Table 2.2.

The values of fluxes after background subtraction show that there is generally very little $24\mu m$ emission coming from the clouds themselves compare to the background level. As a consequence, $24\mu m$ diffuse emission highly underestimate SFR. Figure 2.1 shows the ratio of SFR(YSO count)/SFR(Diffuse, $24\mu m$) versus SFR(YSO count). SFR(Diffuse, $24\mu m$) are much smaller than SFR(YSO count) with the average ratio of SFR(YSO count)/SFR(Diffuse, $24\mu m$) of 203 ± 215, and a median of 113. Figure 2.2 shows the SFR(Diffuse, $24\mu m$) versus SFR(YSO count).

Table 2.2. SFR from diffuse emission of c2d and Gould's Belt survey

Cloud -	Flux[1] (Jy)	SFR (Diffuse, 24 μm) ($M_\odot$ Myr^{-1})	SFR (YSO count) ($M_\odot$ Myr^{-1})	SFR(YSO count)/SFR(Diffuse, 24 μm) -
LUP I	34.2	0.0177	3.2	177
LUP III	107	0.0485	17.0	347
LUP IV	5.81	0.00369	3.0	811
CHA II	47.3	0.0319	6.0	203
SER	204	0.227	56.0	248
PER	2190	1.73	96.2	56
OPH	8620	1.71	72.5	43
CEP	242	0.341	29.5	87
CHA I	70.9	0.0561	22.2	396
CHA III	10.6	0.0104	1.0	100
CrA	286	0.0899	10.2	113
IC5146 1	387	3.97	23.2	5.8
IC5146 2	18.7	0.272	9.5	35
LUP V	48.9	0.0243	11.2	467
LUP VI	66.9	0.0320	10.8	338
MUSCA	0	0.001[2]	3.0	300
SCO	620	0.178 2.5	14	

Notes: [1] These are fluxes inside extinction contours of $A_V = 2$ ($A_V = 6$ for Serpens and $A_V = 3$ for Ophiuchus) after background subtraction. [2] Musca flux is negligible (flux from the cloud before background subtraction is comparable to the average background level). We used lower limit of SFR = 0.001 ($M_\odot$/Myr) for calculation.

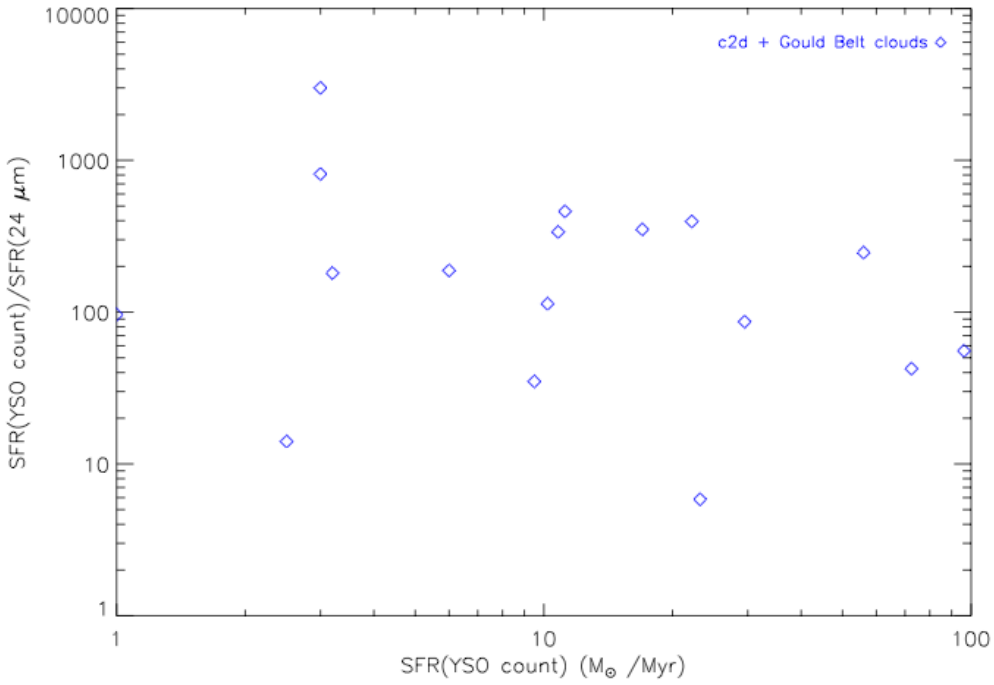

Figure 2.1 Ratio of SFR(YSO count)/SFR(24 μm) over SFR(YSO count) for c2d and Gould's Belt survey. The plot shows the spread in the ratios with average ratio of 203±215.

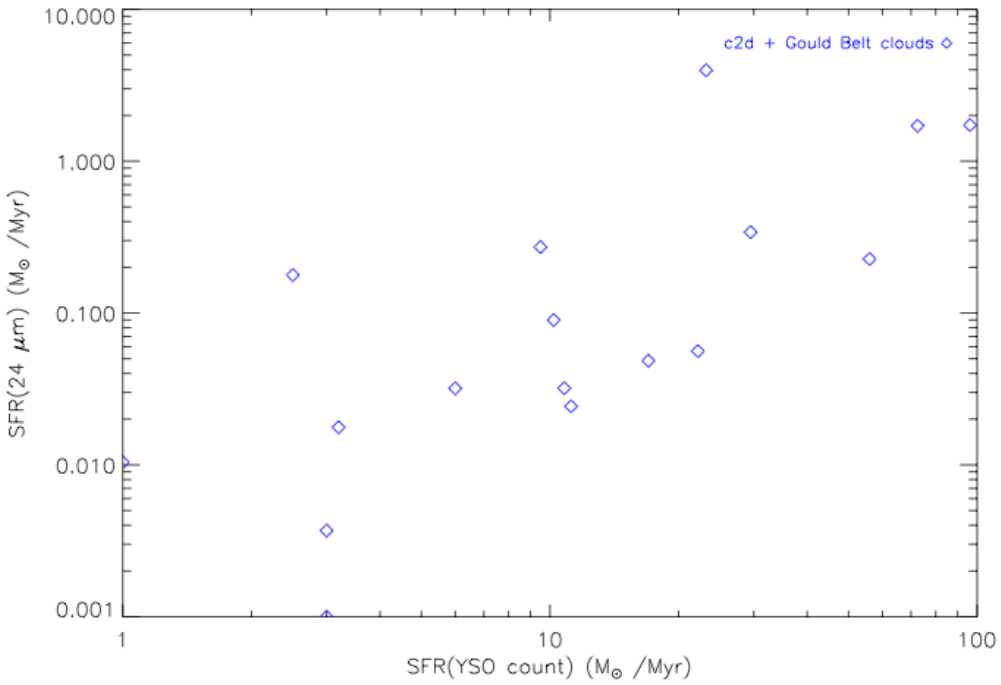

Figure 2.2 Comparison between SFR calculated using 24 μm and SFR from counting YSO for c2d and Gould's Belt survey.

2.3 Contributions from stellar continuum emission

In Calzetti et al. where the 24μm-SFR relation was derived, they studied dust emission at two MIR wavelengths of 8 and 24μm (2007). Since only the dust emission is of interest, stellar continuum emission needed to be subtracted from the flux. The stellar continuum subtraction was performed for the 8μm emission. At 24μm however, contributions to the flux from stellar continuum emission are considered to be negligible. Therefore; the relation was derived without subtracting stellar continuum from the 24μm flux (Calzetti

et al. 2007). To see how much stellar continuum emission contributes to the total flux, we calculated the total stellar flux for the c2d clouds. First, we calculated the flux from all identified objects in the $24\mu m$ MIPS images. Then the YSOs flux was subtracted from the all-object flux to get the non-YSO object flux. The resulting flux should then come mostly from stellar continuum. The results show that stellar continuum contributes little to the total flux for some clouds while the number is more significant in other clouds. The fraction of stellar flux to the total flux is 0.046, 0.81, 0.015, 0.22, 0.71 for the Perseus, Chamaeleon II, Ophiuchus, Serpens, and Lupus clouds respectively. The total flux, YSOs flux, and non-YSO object flux are presented in Table 2.3 for comparison.

Table 2.3 Comparison of diffuse, YSOs, and non-YSOs point sources flux.

Cloud	Total (Jy)	YSOs (Jy)	Non-YSO Objects (Jy)
PER	2190	77.10	81.68
CHA II	47.3	7.93	17.92
OPH	8620	94.16	222.5
SER	204	56.70	47.52
LUP	147	9.45	109.7

Chapter 3

$24\mu m$ emission of high mass star forming regions

So far we have studied the $24\mu m$ emission from the nearby molecular clouds, which only contain low mass star forming regions. These nearby clouds are good samples to study due to the fact that their distances are small enough for us to be able to observe individual YSOs. However, for studying $24\mu m$ as an extra-galactic star formation tracer, high-mass star forming clouds would be more relevant. High mass star forming regions have been observed in many surveys using dense gas tracers and other signposts for high-mass star formation. In this study we used the sample of high mass star forming regions from Wu et al (2010). The sample is a subsample of a large survey by Plume et al. of regions associated with water masers, which are indicators of early phase of massive star formation (Wu et al. 2010). The high mass star forming regions in this sample are massive, dense clumps with average density of about 10^6 cm^{-3} and most masses between $100 - 3000$ M$_\odot$. Most of these clumps have been observed in many molecular line transitions such as CS lines (Plume et al. 1992, 1997; Shirley et al. 2003), HCN 3-2 and HCN 1-0 (Wu et al. 2010). Some of the clumps have also been observed in $350\mu m$ dust continuum emission (Mueller et al. 2002).

3.1 IRAS 25μm emission and total infrared luminosity L_{IR}

Many of the clumps have been observed in the four IRAS bands at wavelengths of 12, 25, 60, 100μm. The data for these clumps can be obtained from IRAS point sources catalogs, which provide photometric data for each IRAS band. The fluxes for the IRAS bands for these clumps are also included in Mueller et al (2002). We used the data on 25μm flux as a substitute for 24μm flux in calculating SFR using the same extragalactic 24μm - SFR relation as the one we used for c2d and Gould Belt clouds. The distances of these clumps are in the order of kpc. Since these clumps are further away from us than the low mass star forming clouds, we cannot resolve the clumps to observe YSO individually. Instead, the total infrared luminosity (8-1000 μm) was used to calculate the SFR for comparison with SFR calculated from 25μm flux. Therefore, the data set in this study includes a total of 32 clumps for which 25μm flux and L_{IR} data are available.

The total infrared luminosity was calculated using the four IRAS bands as follow:

$$L_{IR} = 0.56 \times D^2 \times (13.48 \times f_{12} + 5.16 \times f_{25} + 2.58 \times f_{60} + f_{100}), \quad (3.1)$$

where F_i is the flux in each IRAS band in units of Jy, D is the distance in kpc, and L_{IR} is in the units of $L_\odot$ (Wu et al. 2010). SFRs can be calculated from L_{IR} using the extragalactic relation for starburst galaxies from Kennicutt (1998):

$$SFR(M_\odot year^{-1}) = 4.5 \times 10^{-44} L_{FIR}(ergs^{-1}), \quad (3.2)$$

where L_{FIR} is L_{IR} (8-1000 μm). We calculated SFR using both methods and present the result for all 32 clumps in Table 3.1. A plot of SFR(L_{IR})/SFR(24μm) over SFR(L_{IR}) for all the clumps are shown in Figure 3.1, and a plot of SFR(24μm) versus SFR(L_{IR}) is shown in Figure 3.2. The two SFRs are comparable to each other with the average ratio of SFR(L_{IR})/SFR(25μm) = 0.896±0.663. The median is 0.613±0.663.

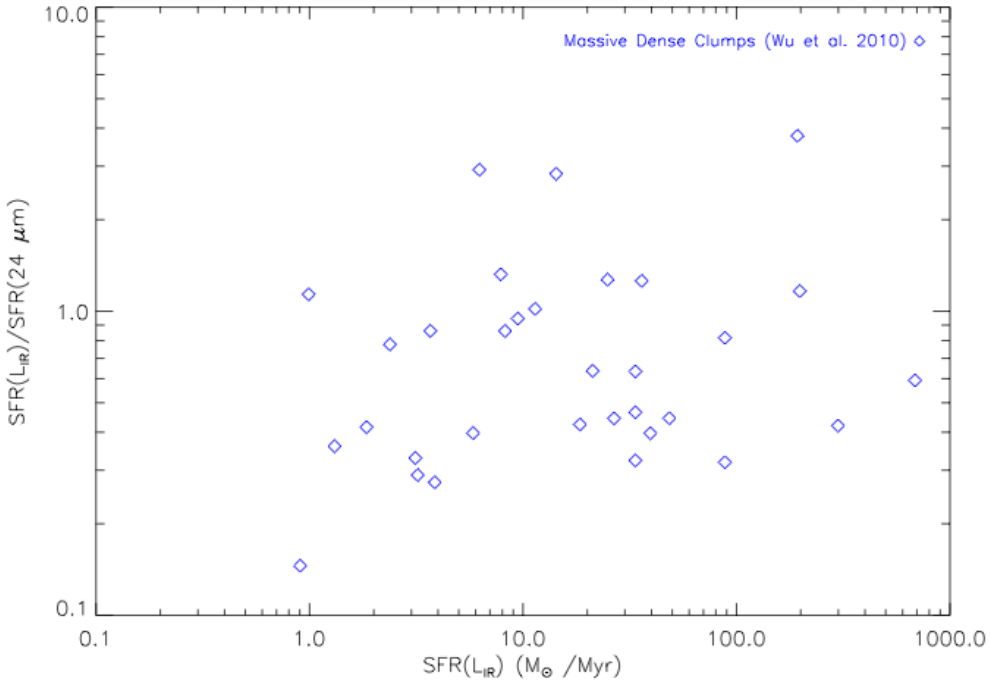

Figure 3.1 Ratio of SFR(L_{IR})/SFR(24 μm) over SFR(L_{IR}) for Massive dense clumps. The plot shows the spread in the ratios with average ratio of 0.896±0.663.

Table 3.1. Massive Dense Clump Sample

Object -	Distance (kpc)	$Flux_{25\mu m}$ (Jy)	$Log(L_{IR})$ ($L_\odot$)	$SFR(25\mu m)$ ($M_\odot$ Myr^{-1})	$SFR(L_{IR})$ -	$SFR(L_{IR})/SFR(25\mu m)$ -
G123.07-6.31	2.2	13	3.76	0.872	0.991	1.14
W3(OH)	2.4	670	5.09	33.3	21.2	0.636
S231	2.3	75	4.03	4.45	1.85	0.415
S235	1.6	226	3.72	6.21	0.904	0.146
S241	4.7	11.8	4.14	3.06	2.38	0.777
S252A	1.5	77	4.56	2.14	6.25	2.92
RCW142	2	281	4.82	11.2	11.4	1.02
W28A2(1)	2.6	2190	5.45	109	48.5	0.445
M8E	1.8	289	4.26	9.51	3.13	0.330
G10.60-0.40	6.5	148	6.05	51.1	193	3.78
G12.42+0.50	2.1	253	4.27	11.1	3.21	0.290
G12.89+0.49	3.5	45	4.66	5.95	7.87	1.32
G13.87+0.28	4.4	478	5.29	72.2	33.6	0.465
W33A	4.5	371	5.19	60.1	26.7	0.444
G14.33-0.64	2.6	56	4.33	4.27	3.68	0.862
G19.61-0.23	4	407	5.29	53.0	33.6	0.634
G23.95+0.16	5.8	395	5.36	99.5	39.5	0.397
G24.49-0.04	3.5	81	4.74	10.0	9.46	0.946
W43S	8.5	1679	6.24	711	299	0.421
G31.41+0.31	7.9	52	5.32	28.6	36.0	1.26
G35.58-0.03	3.5	9.57	4.68	9.57	8.24	0.861
G48.61+0.02	11.8	170	6.06	170	198	1.16
W51M	7	4344	6.6	1158	686	0.592
S87	1.9	425	4.53	14.7	5.84	0.397
S88B	2.1	1185	5.03	43.6	18.5	0.423
ON 1	6	58.8	5.16	19.6	24.9	1.27
ON 2S	5.5	481	5.71	108	88.3	0.818
S106	4.1	2510	5.71	277	88.3	0.319
BFS 11-B	2	79	3.88	3.64	1.31	0.359
CepA	0.73	860	4.92	5.05	14.3	2.84
S158	2.8	1780	5.29	104	33.6	0.323
S157	2.5	233	4.35	14.1	3.86	0.273

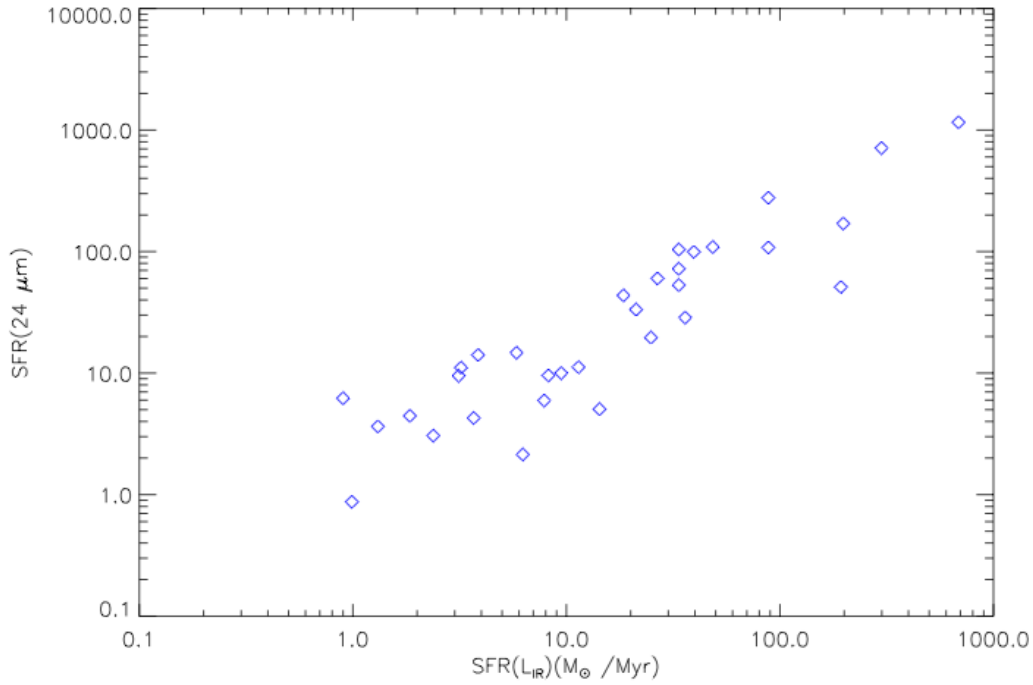

Figure 3.2 Comparison between SFR calculated using 25 μm and SFR from total infrared luminosity .

Chapter 4

Analysis

From the results for c2d and Gould's Belt survey clouds, the SFRs from $24\mu m$ do not agree well with SFRs from YSO counts. The ratios of SFR(YSO count)/SFR(Diffuse, $24\mu m$) are shown in Figure 2.1. SFRs from YSO $24\mu m$ flux are much smaller than SFR from YSO count by many orders of magnitude. Even when we include the diffuse emission in our calculations of total $24\mu m$ flux, there are still large discrepancies between SFRs calculated from the two methods. The reason for the discrepancies can be seen from the diffuse flux calculation. Most of the emission in the $24\mu m$ images is background emission, which means that most of the emission detected did not come from within star forming regions. The emission should be contributed by dust grains that have been heated by interstellar radiation field. Comparing extinction contours with the $24\mu m$ images shows that most of the extended $24\mu m$ emission does not correspond to regions of high extinction. Since extinction maps trace regions of star formation fairly well (see detail study in Heiderman 2010), this result means that $24\mu m$ emission does not generally trace star forming regions. Figure 4.1 shows the MIPS $24\mu m$ image of Ophiuchus cloud overlaid with extinction contours of A_V = 2, 6, and 10. Ophiuchus cloud is one of the clouds with high diffuse flux compare to YSO flux and one where $24\mu m$

emission has some correlation with extinction level. Lupus I cloud on the contrary has a very low ratio of SFR(YSO)/SFR($24\mu m$). The image of Lupus cloud is shown in Figure 4.2 with overlaid extinction contours of $A_V = 2$, 4, and 6. For Lupus I, the $24\mu m$ emission does not correlate with extinction level, and most of the diffuse flux is comparable to the background flux. The results indicate that for these low-mass star forming regions, $24\mu m$ emission does not trace SFR. Stronger stellar radiation field might be needed to heat the dust high enough to emit significantly in the $24\mu m$ band.

As for the case of high mass star forming clumps, the SFR($24\mu m$)s agree well with SFR(L_{IR})s with the average ratio of SFR(L_{IR})/SFR($24\mu m$) = 0.896 ± 0.663. The plot of the SFR ratios for all clumps is shown in Figure 3.1. There are some scatters in the data and the averaged SFR(24 μm) is slightly less than the averaged SFR((L_{IR}). Between the low mass and high mass star forming regions we studied, $24\mu m$ emission from high mass star forming regions seems to trace SFR fairly well while $24\mu m$ emission does not trace SFR at all in low mass star forming regions. This result is to be expected since the assumption in using $24\mu m$ as a SFR tracer is that the emission should come mostly from dust that has been heated by photons from high mass stars. Therefore, for low mass star forming regions, the heating of the dust from YSOs is not high enough for the dust emission to be noticeably above the background emission. We would then expect that $24\mu m$ would not trace SFR in low mass star forming regions, which is what our results indicate.

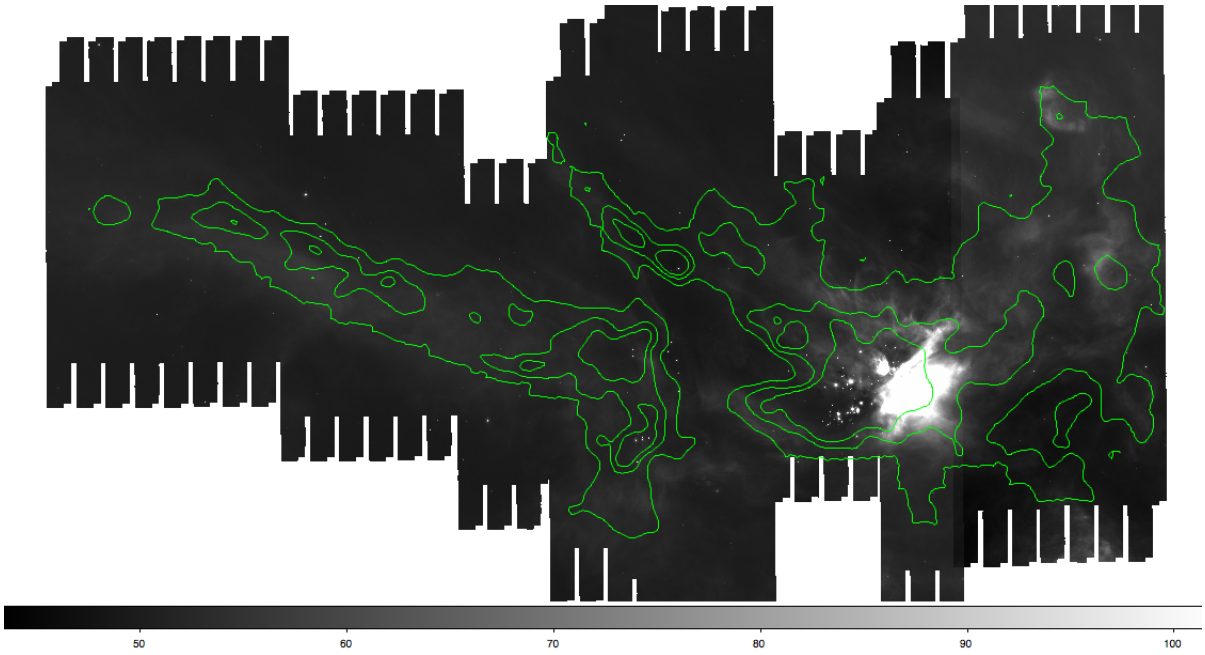

Figure 4.1 MIPS 24μm image of Ophiuchus cloud with overlaying of extinction contour level of $A_V = 2$, 6, and 10.

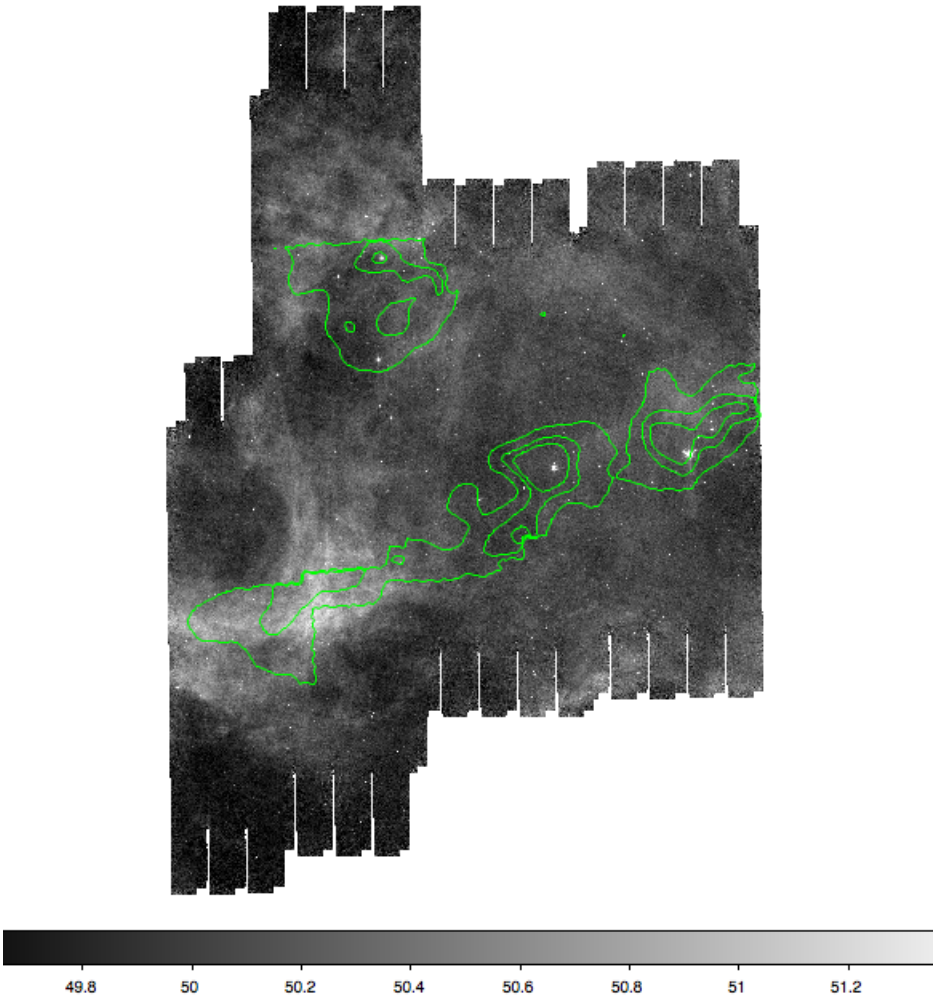

Figure 4.2 MIPS 24μm image of Lupus I cloud with overlaying of extinction contour level of $A_V = 2$, 4, and 6

Chapter 5

Summary

We studied three groups of star forming clouds in the Milky Way: 5 clouds from Spitzer c2d Legacy survey, 10 clouds from Gould Belt survey, and 32 massive dense clumps. We determined the total diffuse $24\mu m$ emission for each cloud and calculated the corresponding SFR using extragalactic relation from Calzetti (2007). Then the resulting SFRs were compared with SFRs calculated using the method of counting number of YSOs for c2d and Gould Belt clouds and using L_{IR} for massive dense clumps. The comparison shows quite a good correlation for the massive dense clumps, which are high-mass star forming regions, with the average ratio of $SFR(L_{IR})/SFR(25\mu m) = 0.896 \pm 0.663$. The result for low-mass star forming clouds (c2d and Gould Belt) shows very little to no correlation between $L_{24\mu m}$ and SFR(YSO count). Comparing $24\mu m$ images with extinction maps shows that a significant portion of $24\mu m$ emission does not come from star-forming regions in the cloud.

References

Alonso-Herrero, A., Rieke, G. H., Rieke, M. J., et al. 2006, ApJ, 650, 835

Bigiel, F., Leroy, A., Walter, F., et al. 2008, AJ, 136, 2846

Calzetti, D., Kinney, A. L., Storchi-Bergmann, T. 1994, ApJ, 429, 582

Calzetti, D., et al. 2007, ApJ, 666, 870

Condon, J. J., 1992, ARAA, 30, 575

Draine, B. T., Anderson, N., 1985, ApJ, 292, 494

Draine, B. T., Dale, D. A., Bendo, G., et al. 2007, ApJ, 663, 866

Evans, N. J., II, et al. 2003, PASP, 115, 965

Evans, N. J., II, et al. 2009, ApJ, 181, 321

Gao, Y., Solomon, P. M., 2004, ApJ, 606, 271

Gutermuth, T. L., Bourke, L. E., Allen, P. C., et al. 2008, ApJ, 673, 151

Heiderman, A., Evans, N. J., et al. 2010, ApJ, 723, 1019

Helou, G., Roussel, H., Appleton, P. 2004, ApJS, 154, 253

Kennicutt, R. C., 1998, ApJ, 498, 541

Kennicutt,R. C. 1998, ApJ, 498, 541

Kennicutt, R. C., 2003, The Astronomical Society of the Pacific, 115, 928

Kinney, A. L., Bohlin, R. C., Calzetti, D., Panagia, N., Wyse, R. F. G. 1993, ApJS, 86, 5

Kirk, J. M., Ward-Thompson, D., Francesco, J., et al. 2009, ApJ Supplement, 185, 198

Lada, C. J., 2010, ApJ, 724, 687

Plume, R., Jaffe, D. T., Evans, N. J. II, Martin-Pintado, J., Gomez-Gonzalez, J. 1997, ApJ, 476, 730

Rahman, N., Bolatto, A. D., Wong, T., 2011, 730, 72

Rosie Chen, C-H., Indebetouw, R., Chu, Y-H., et al. 2010, ApJ, 721, 1206

Verley, S., Corbelli, E., Giovanardi, C., Hunt, L. K., 2009, A&A, 493, 453

Wu, H., Cao, C., Hao, C., et al. 2005, ApJ, 632, 79

Wu, Jingwen., Evans, N. J., Shirley, Y., 2010, ApJ Supplement,188, 313

This thesis was typeset with LaTeX[†] by the author.

[†]LaTeX is a document preparation system developed by Leslie Lamport as a special version of Donald Knuth's TeX Program.